HAL open science

A new method for measuring nanoparticle diameter from a set of SEM images using a remarkable point

Loïc Crouzier, Alexandra Delvallee, Sébastien Ducourtieux, Laurent Devoille, Christophe Tromas, Nicolas Feltin

▶ **To cite this version:**

Loïc Crouzier, Alexandra Delvallee, Sébastien Ducourtieux, Laurent Devoille, Christophe Tromas, et al.. A new method for measuring nanoparticle diameter from a set of SEM images using a remarkable point. Ultramicroscopy, 2019, 207, pp.112847. 10.1016/j.ultramic.2019.112847 . hal-02316584

HAL Id: hal-02316584

https://hal.science/hal-02316584v1

Submitted on 20 Jul 2022

HAL is a multi-disciplinary open access archive for the deposit and dissemination of scientific research documents, whether they are published or not. The documents may come from teaching and research institutions in France or abroad, or from public or private research centers.

L'archive ouverte pluridisciplinaire **HAL**, est destinée au dépôt et à la diffusion de documents scientifiques de niveau recherche, publiés ou non, émanant des établissements d'enseignement et de recherche français ou étrangers, des laboratoires publics ou privés.

Distributed under a Creative Commons Attribution - NonCommercial 4.0 International License

Version of Record: https://www.sciencedirect.com/science/article/pii/S0304399119302566
Manuscript_a659cf37751baef73bc6a34cc495226c

FA new method for measuring nanoparticle diameter from a set of SEM images using a remarkable point

Loïc Crouzier[1,2], Alexandra Delvallée[1], Sébastien Ducourtieux[1], Laurent Devoille[1], Christophe Tromas[2], Nicolas Feltin[1]

[1] *Laboratoire National de métrologie et d'Essais - Nanometrology, 29 avenue Hennequin, 78197 Trappes Cedex (France)*

[2] *Institut Pprime Département Physique et Mécanique des Matériaux – 11 Bd Marie et Pierre Curie, 86962 Futuroscope Chasseneuil (France)*

Corresponding author: Loic.Crouzier@lne.fr

Abstract

Scanning Electron Microscopy (SEM) is considered as a reference technique for the determination of nanoparticle (NP) dimensional properties. Nevertheless, the image analysis is a critical step of SEM measuring process and the initial segmentation phase consisting in determining the contour of each nano-object to be measured must be correctly carried out in order to identify all pixels belonging to it. Several techniques can be applied to extract NP from SEM images and evaluate their diameter like thresholding or watershed. However, due to the lack of reference nanomaterials, few papers deals with the uncertainty associated with these segmentation methods. This article proposes a novel approach to extract the NP boundaries from SEM images using a remarkable point. The method is based on the observation that, by varying the electron beam size, the secondary electron profiles crosses each other at this point. First, a theoretical study has been performed using Monte Carlo simulation on silica NP to evaluate the robustness of the method compared with more conventional segmentation techniques (Active Contour or binarization at Full Width at Half-Maximum, FWHM). The simulation results show especially a systematic discrepancy between the NP real size and the measurements performed with both conventional methods. Moreover, generated errors are NP size-dependent. By contrast, it has been demonstrated that a very good agreement between measured and simulated diameters has been obtained with this new technique. As an example, this method of the remarkable point has been applied on SEM images of silica particles. The quality of the segmentation has been shown on silica reference nanoparticles by measuring the modal equivalent projected area diameter and comparing with calibration certificate. The results show that the NP contour can be very accurately delimited with using this point. The measurement uncertainty has been also reduced from 4.3 nm (k = 2) with conventional methods to 2.6 nm (k = 2) using the remarkable point.

Key words

SEM, Monte Carlo modeling, nanoparticle, diameter measurements

© 2019 published by Elsevier. This manuscript is made available under the CC BY NC user license
https://creativecommons.org/licenses/by-nc/4.0/

Funding

This research did not receive any specific grant from funding agencies in the public, commercial, or not-for-profit sectors.

1. Introduction

Scanning Electron Microscopy (SEM) is considered as a reference method for the determination of the nanoparticles (NP) dimensional properties and was defined as the most reliable method in the NanoDefine project to assess whether a material is a nanomaterial according to the definition by the EC [1]. In SEM technique, the image of a sample is obtained from the secondary electrons (SE) generated through the inelastic interaction occurring between electron beam and atoms of the sample surface. Thus, if SE have sufficient energy, they can escape from the sample surface and be collected by a detector. The dimensional properties of a NP population can be deduced from the images generated by SE. As a result, the nanoparticle size is determined from data included in XY plane and generally defined through the equivalent projected area diameter (D_{eq}) measurement. In contrast, in SEM images, data along Z-axis provide no metrological information and represent signal intensity displayed in grey level [2,3].

But, prior to measuring D_{eq} of each NP on SEM images, segmentation step must be carried out in order to correctly identify all pixels belonging to NP. In general way, for this purpose, there are two different methods based either on the application of a local or global threshold followed by a binarization process of the image or on the implementation of algorithms (for instance, watershed method) capable of automatically determining more or less accurately the contours around the nano-objects of interest [4,5]. In the case of the first method involving a binarization step, D_{eq} is deduced from the measurement of NP surface area on binary image. But, due to the convolution of NP with the incident electron beam assumed to be Gaussian, the NP edges observed in the SE profile are not perfectly vertical (*Figure 1*). As a consequence, the selection of the threshold value will have a significant impact on the measurement result [6,7]. It is generally accepted that two approaches can be used to minimize measurement errors. The first one consists in applying the threshold at half-maximum of NP profiles [2] and gives an equivalent diameter called in this article $D_{eq\text{-}HM}$. The second one, called active contour or snakes, locates the inflection points on NP SEM profiles [8] and can be used to determine their contours (*Figure 1*) [9] giving also an equivalent diameter called here $D_{eq\text{-}ActiveContour}$.

Furthermore, studies have shown that several SEM imaging parameters can modify the raw signal level or NP profile shape drawn from SE images [3,10]. Two parameters can be mentioned in particular: the electron beam size and the accelerating voltage. Both are well-known for directly impacting the SEM signal. Indeed, the size and the shape of the e-beam induce a convolution effect between sample and e-beam, tending to distort the SEM profile. Moreover, the e-beam size depends on instrument performances and is directly linked to the accelerating voltage [11,12]. The value of this parameter is important to know because the electron beam size has been recently evaluated as the main component of the uncertainty budget associated with NP SEM measurements [3]. Indeed, the contribution of this component reached roughly 80 % of expanded uncertainty associated with the silica NP size measurement by SEM. Several methods can be used to estimate it [13,14]. But, no metrological characterization has been undertaken so far, to the best of our knowledge.

As a consequence, the question is whether the changes of the electron beam size as well as the choice of the accelerating voltage can influence the optimal position on the SEM profile where the measurements of D_{eq} must be carried out to minimize errors and make it reliable. In that respect, the use of segmentation methods

independent of these parameters could make it possible to drastically reduce the uncertainty associated with the diameter measurement of NP population by SEM. Indeed, the expanded uncertainty associated with the mean diameter of silica nanoparticle population (FD 304, indicative value 27.8 nm) was found to be 4.84 nm [15].

In order to evaluate the uncertainty linked to the electron beam size and associated with the NP size measurements using SEM, Monte Carlo simulation of electron trajectories in material has been used. From these results, we observe that the simulated signals obtained at different probe sizes intersect at a single point near to the object boundary. This point is also observed in other studies, but has not been fully exploited until now [16,17,18]. These papers focused, through a Monte Carlo approach, on the impact of beam size variation on critical dimension measurements using SEM [16], NP diameter measurements using TSEM [17], or Au layer thickness measurements using backscattering electron (BSE) signal in SEM [18]. Therefore, in this paper, we propose to use this remarkable point to determine NP contour on SEM images and, thus, determine D_{eq} with a reduced uncertainty. Indeed, the main advantage of this method is that the position of this point is independent of the electron beam size. In order to implement it, we propose a novel approach consisting in combining a set of images of the same object taken with different electron beam size by modifying the focus.

However, the proof of concept of this method requires several validation steps. Firstly, the effect of electron beam size on $D_{eq\text{-}HM}$ and $D_{eq\text{-}ActiveContour}$ has been studied theoretically using Monte Carlo simulation. In order to only take into account the effect of this parameter, the accelerating voltage is kept constant for all study. Secondly, the novel approach has been implemented by determining the equivalent diameter ($D_{eq\text{-}CurveCrossing}$), measured through this remarkable point on simulated profiles. The values of $D_{eq\text{-}CurveCrossing}$ have been compared with simulated diameter and also with equivalent diameter obtained by using half maximum thresholding and the Active Contour method. Finally, the three segmentation methods have been compared experimentally on silica reference nanoparticles images obtained by SEM. The uncertainties budgets associated with each segmentation techniques have been evaluated using the method described in [3].

Figure 1 : Nanoparticle equivalent diameter measurement principle, using Active Contour and FWMH methods, from a SEM image

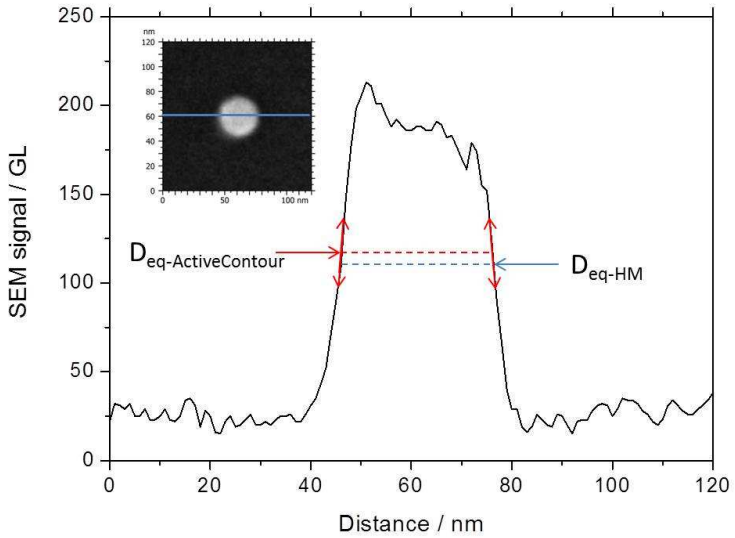

2. Materials and method

2.1. Sample

The measurements presented in this article have been performed on SiO_2 nanoparticle deposited from suspension on silicon substrate. The suspension used in this study (ERM – FD101b) is a certified reference sample provided by the Joint Research Centre (JRC). The latter is a bimodal population of silica NP with a number-weighted modal area equivalent diameter value specifically certified for electron microscopy techniques and given to be (83.7 ± 2.2) nm (coverage factor k=2) [19]. The area equivalent diameter (D_{eq}) corresponds to the diameter of a circle which would have the same projected surface area as the imaged nano-object. Moreover, in this study, only the certified mode has been taken into account by only counting particles with an area equivalent diameter larger than 60 nm as mentioned by the certification report [19].

NP suspension was diluted in water and deposited on silicon substrates through the spin coating method detailed in [2]. This method generally provides a population of nanoparticles well-dispersed on the substrate. However, as the silica NP and substrate are both negatively charged, the NP adhesion is too weak. This usually leads to a very limited number of particles deposited on the substrate and makes difficult the measurements. That is the reason why the silicon substrate has been chemically functionalized to promote the bonding between the nanoparticles and the surface. This was achieved by depositing a thin layer of poly-$_L$-lysine (PLL) on the substrate surface by using spin coating method [20,21].

2.2. SE profiles simulation using Monte Carlo modelling

The SEM principle is based on the interaction between the incident electron beam and the constituting atoms of the sample surface. These interactions are the result of a series of inelastic or elastic scattering processes within the sample. In order to model the SEM signal, it is necessary to simulate electrons trajectories in the course if these interactions until they either lose their kinetic energy or leave from the specimen surface.

JMONSEL (Java Monte Carlo Simulation of Secondary Electron) simulator has been used in this purpose. This latter is based on NISTMonte model developed for providing Monte Carlo simulation of electron transport in complex sample geometries [22]. The JMONSEL package includes multiple components related to the beam/sample interaction, electron probe properties, sample geometry or SE detection system. All of these components have been already described in previous studies [23,24,25,26].

In the context of this paper, the simulations have been conducted onto perfectly spherical silica NP deposited on silicon substrate. To assess the viability of the method in the nanoscale range, they have been performed on several silica particles with modeled diameter ($D_{JMONSEL}$) ranging from 15 nm to 100 nm with constant step of 1 nm. For each $D_{JMONSEL}$, a scanning line, consisting of 121 points separated with 1 nm step size is generated. For each point, 4000 electrons trajectories are simulated. For each incident electron, several secondary electron are generated inside the NP and can possibly extracting from the nano-object (*Figure 2-a*). At a single point, SE yield is calculated as the ratio of the collected SE to that of the number of primary electrons. The scanning along the NP diameter makes it possible to establish a theoretical SE profile as shown in *Figure 2-b*. On a standard computer, the time need to perform a linescan is estimated to be equal to 1 hour.

For each modeled NP diameter, several profiles have been generated according to the electron beam size. The voltage value is equal to 3 kV for all simulations and corresponds to SEM voltage levels generally set for imaging silica NP populations [3]. At this accelerating voltage, the corresponding electron beam size can be roughly estimated using manufacturer specification (see section 2.3.1 for SEM details). The probe size (R_{50}) is about 1.7 nm at 1 kV accelerating voltage and 1.0 nm at 15 kV for a working distance of 2 mm. R_{50} value here represents the radius that encircles 50% of the electron beam charge [11]. Consequently, three beam sizes have been selected for modeling NP secondary electron profiles: 1.5 nm, 3 nm and 5 nm. In JMONSEL, these values correspond to the standard deviation of the Gaussian electron beam. The 1.5 nm size is consistent with the experimental value relating to the specifications of the Zeiss Ultra Plus microscope used in this study. The others one has been arbitrary chosen.

Figure 2: (a) Electron trajectories inside the NP. Blue lines corresponds to primary electrons trajectories, red lines to trajectories of SE generated inside the nano-object (b) SE profile of silica particle deposited on silicon substrate obtained from JMONSEL simulation

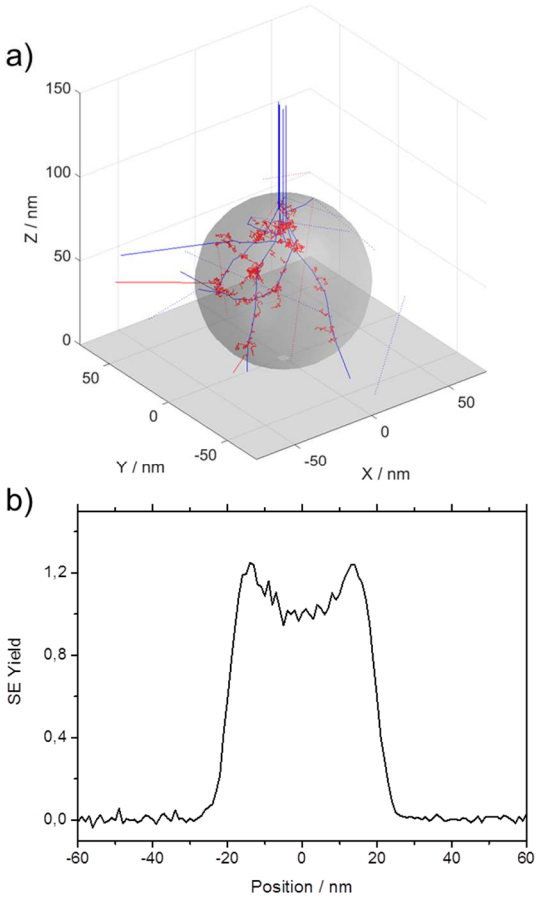

2.3. SEM measurements

2.3.1. Experimental parameters

Measurements have been performed using Field Emission Gun (FEG) SEM Zeiss Ultra plus equipped with Gemini column. In order to perform high resolution imaging, in-lens detector located inside the column has been used. Its geometric position, directly in the electron beam path, coupled with electrostatic and electromagnetic lens allows high detection efficiency of SE [27]. The diaphragm aperture size has been fixed to 30 µm. The whole system is placed on a massive concrete block dissociated from the building in order to avoid vibrations issues. In order to prevent contamination effect, the sample has been left in high vacuum (6.10^{-7} mbar) within the chamber 24 hours before the measurement.

The comparability of the images obtained at different beam sizes requires keeping all other parameters constant. The image resolution has been set at 2048 x 1536 pixels for all measurements. Images have been captured using x40 000 magnification in order to obtain a sufficient number of particles per images according to ISO 13322-1 recommendation [4]. This leads to a 1.4 nm pixel size for all images. “Line integrate” image acquisition mode has been used in this study. Each scanning line is repeated 20 times to reduce noise level of the image.

2.3.2. Experimental procedure to modify the electron beam size

The electron beam diameter is mainly controlled using condenser lenses [28]. These lenses are located above the column aperture. When the electron passes though the latter, it converges at a single point and then widens again before crossing the column aperture. By this way, non-directional electrons are filtered out. Finally, electron beam is focused once again on the sample surface by the objective lens located below the aperture.

Thus, as shown in *Figure 3*, the size of the electron beam which lands on the sample surface depends on the position of the focal plane. On our SEM, the position of this latter is adjusted experimentally using "Focus" scroll button. Consequently, in our study, images have been acquired successively with different focus. Moreover, between each image acquisition on the same sample area, the electron beam is blanked in order to reduce sample charging and "Focus" button is randomly scrolled. For the same area, three images have been acquired with the first one done with optimized focus settings (*Figure 3*). The images which are not taken in the focal plane are objectively blurred.

Because the method requires performing three images on the same sample area, contamination phenomenon could occur. This contamination is mainly due to adsorbed organic molecules on the sample surface, formed during e-beam scanning. Nevertheless, in order to minimize this effect, the sample is maintained in high vacuum within the chamber from 24 hours to 48 hours before the measurement. Moreover, the exposure of the sample to the e-beam is reduced by (1) adjusting the settings outside the area of interest and (2) blanking the beam during the focus modification between each image acquisition. As a result, the total exposure time to the e-beam is limited to 90 seconds regarding image acquisition parameters.

Figure 3: Principle of the SEM beam size modification method and corresponding SEM images obtained on the same sample area

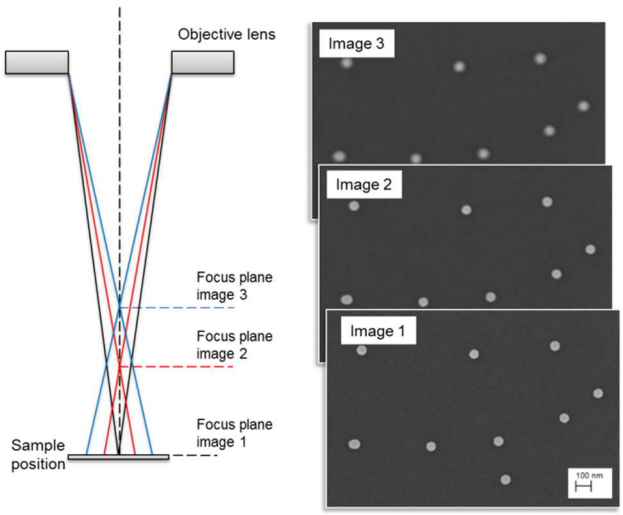

2.4. Data processing

2.4.1. Determination of $D_{eq\text{-}CurveCrossing}$, $D_{eq\text{-}ActiveContour}$ and $D_{eq\text{-}HM}$ on simulated profiles using Matlab routine

For the same silica NP diameter ($D_{JMONSEL}$) set on JMONSEL, three different line scans are simulated using three different beam size (standard deviation of the Gaussian electron beam equal to 1.5 nm, 3 nm and 5 nm, respectively). In order to be directly compared, each line scan is normalized between the maximum point on the profile and the average point corresponding to the substrate signal. The corresponding normalized SE profiles of the same NP diameter using three different beam size is present in *Figure 4-a*.

From the normalized profiles, the position where curves crosses each other is determined by calculating the standard deviation of the intensity level for each point between the three profiles (*Figure 4-b*). Thus, theoretically, at this "curve crossing" point, the standard deviation must be null or minimal. Moreover, because of the NP/ Gaussian Beam convolution, standard deviation must be maximal around this point. Consequently, on standard deviation profile, $D_{eq\text{-}CurveCrossing}$ is determined to be equal to the distance between the two local minima using Matlab routine.

As the profile has been normalized previously, $D_{eq\text{-}HM}$ and $D_{eq\text{-}ActiveContour}$ correspond respectively to the distance between both points having intensity closest to 0.5 and between both inflection points on each side of the normalized SE curve.

Figure 4: (a) Normalized SE profiles of silica NP with 40 nm diameter obtained at different beam size using JMONSEL (b) Corresponding standard deviation curve

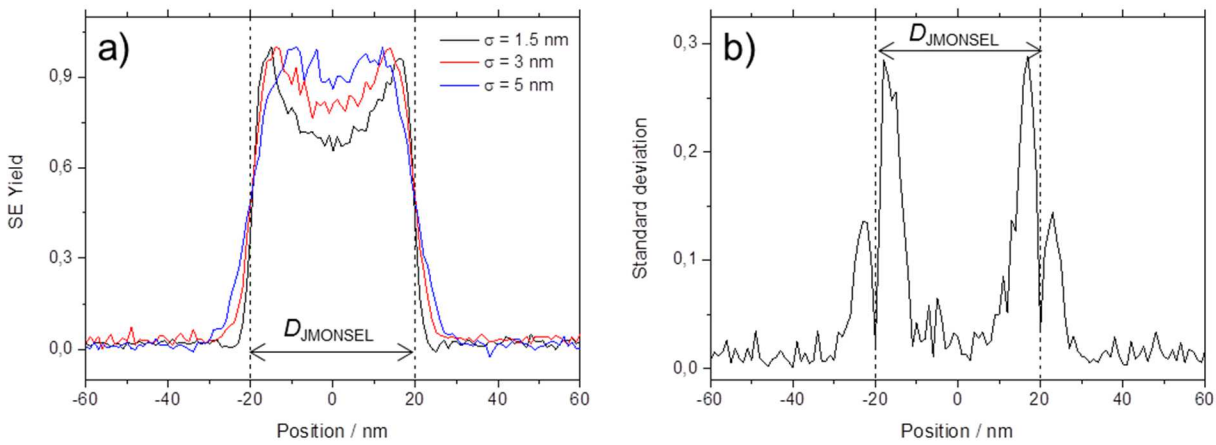

2.4.2. Determination of $D_{eq\text{-}CurveCrossing}$, $D_{eq\text{-}ActiveContour}$ and $D_{eq\text{-}HM}$ on SEM images using Matlab routine

In order to extract NP contours on SEM images using "Crossing curves" method, a specific Matlab routine has also been developed. The aim of this routine is to locate the position of the local minima as explained in section 2.4.1. To do this, a standard deviation image is created from the combination of images of the same area at different beam size and local minima are localized on it. This Matlab routine includes several steps. First, for each image, particles are localized and indexed by a rough threshold. Then, a thumbnail is created for each NP (*Figure 5*). In order to be directly compared to each other, they are centered on the NP centroids. The direct comparison on the thumbnails makes it possible to ignore instrument drifts present between each image

acquisition. At this stage, for each particles, three thumbnails are created corresponding to the three images acquired with different focus planes.

Then, a standard deviation image is created (*Figure 5*) using the thumbnails of the same NP, obtained on each image. This one is obtained by calculating the standard deviation pixel by pixel between each thumbnail of the same particle. The local minima are then localized on the standard deviation image. The NP boundaries are obtained by setting the pixel corresponding to the local minima to be equal to 1 on a binary image. By filling the area inside the NP boundary on the binary image, the area can be determined and thus $D_{eq\text{-}CurveCrossing}$ too.

Moreover, the Matlab routine also includes an Active Contour algorithm in order to determine $D_{eq\text{-}ActiveContour}$ for each NP. The calculation of each $D_{eq\text{-}HM}$ is also taken over by the routine. As the nanoparticle profile of the thumbnail image has been previously normalized, the binarization is carried out with half maximum threshold exactly equal to 0.5. Both methods are applied only on the focused images.

Thanks to the binarization process, two points, called p_1 and p_2 are obtained on each side of the profile. These points (pixels) correspond to the intersection of the profile with the applied threshold. Regarding others methods, p_1 and p_2 correspond to the inflexion points or the position where curves crosses each other at each side of the SE profile for Active Contour and "Curve-Crossing" methods, respectively. Thus, D_{eq} corresponds to the distance between these pixels and can be described as $D_{eq} = p_2 - p_1$ with p_2 and p_1 the position (pixel) of the right and left points on the profile, respectively. The uncertainty associated to the position of these points is directly linked to the pixel size. Assuming a uniform law and with a the pixel size set as 1 nm, the uncertainties associated with p_2 and p_1 positions $u(p_2)$ and $u(p_1)$ can be describe as:

$$u(p_1) = u(p_2) = \frac{a}{2}\frac{1}{\sqrt{3}} = \frac{0.5}{\sqrt{3}} = 0.3\ nm \tag{1}$$

Thus, the uncertainty associated with D_{eq} measurement on the profiles $u(D_{eq})$ is equal to:

$$u(D_{eq}) = \sqrt{u(p_1)^2 + u(p_2)^2} = \sqrt{2}\frac{0.5}{\sqrt{3}} = 0.4\ nm \tag{2}$$

Figure 5: Principle of extraction of $D_{eq\text{-}CurveCrossing}$ on SEM images taken with different beam width using a Matlab routine

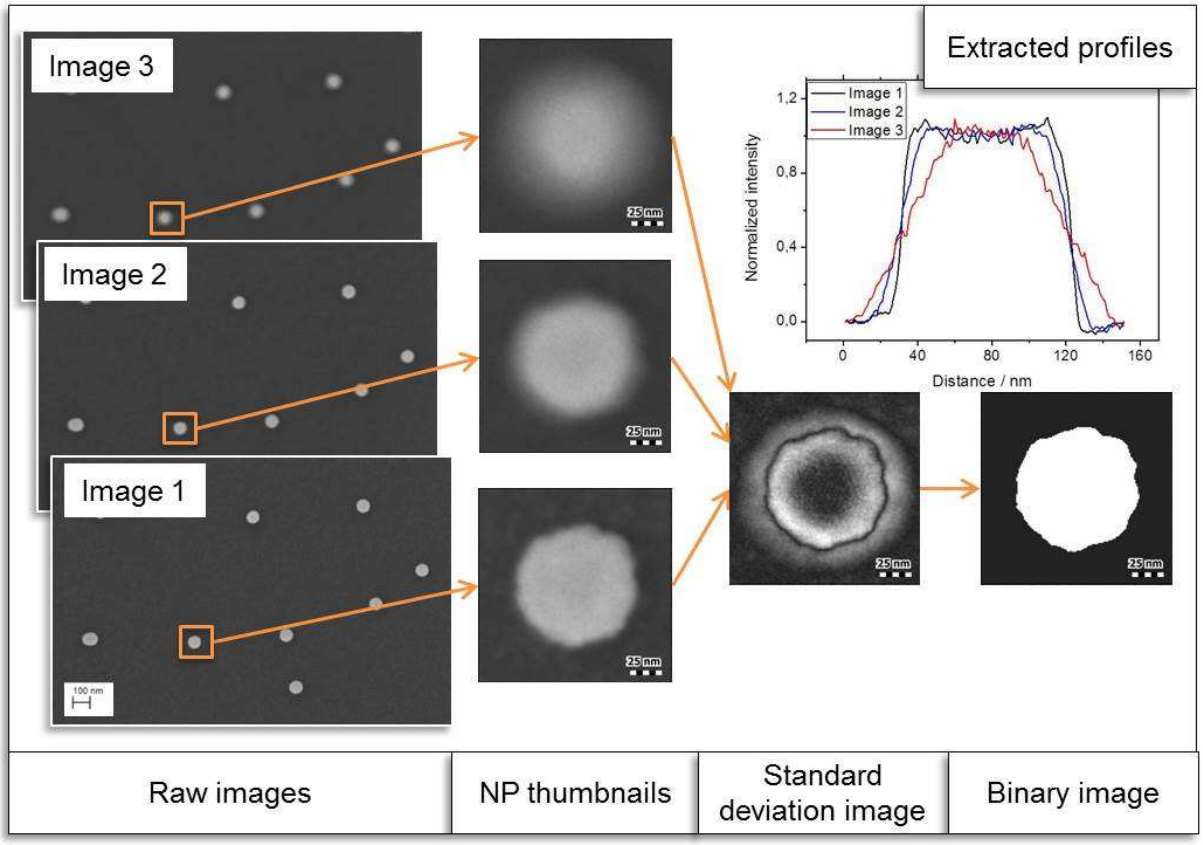

3. Results and discussions

3.1. Monte Carlo modelling

3.1.1. Effect of electron Gaussian beam size and nanoparticle size dependence on $D_{eq\text{-}ActiveContour}$ and $D_{eq\text{-}HM}$

The effect of beam size on $D_{eq\text{-}ActiveContour}$ and $D_{eq\text{-}HM}$ measurements has been investigated using Monte Carlo modelling. The e-beam size is a key parameter that has a large contribution in NP diameter measurement uncertainty by SEM [3] but its value is difficult to be evaluated. The measurement protocol, described in section 2.4.1, has been applied by varying electron beam size. From the profiles obtained using modelling, the relative differences $\overline{D_{eq-ActiveContour}}$ and $\overline{D_{eq-HM}}$ have been calculated on the whole nanoscale range and are presented in *Figure 6*. These relative differences with respect to the input value used in the model ($D_{JMONSEL}$) have been defined as following:

$$\begin{cases} \overline{D_{eq-CurveCrossing}} = \dfrac{D_{JMONSEL} - D_{eq-CurveCrossing}}{D_{JMONSEL}} \\ \overline{D_{eq-ActiveContour}} = \dfrac{D_{JMONSEL} - D_{eq-ActiveContour}}{D_{JMONSEL}} \\ \overline{D_{eq-HM}} = \dfrac{D_{JMONSEL} - D_{eq-HM}}{D_{JMONSEL}} \end{cases} \tag{3}$$

The relative uncertainty associated with each $\overline{D_{eq}}$ can be determined using (2) and is equal to:

$$u(\overline{D_{eq}}) = \frac{u(D_{eq})}{D_{JMONSEL}} \tag{4}$$

Figure 6: Relative difference between $\overline{\boldsymbol{D_{eq}}}$ for silica particles with diameter ranging from 15 nm to 100 nm as a function of beam size determined using (a) Active Contour and (b) Half Maximum segmentation techniques. For all measurements, accelerating voltage is equal to 3 kV.

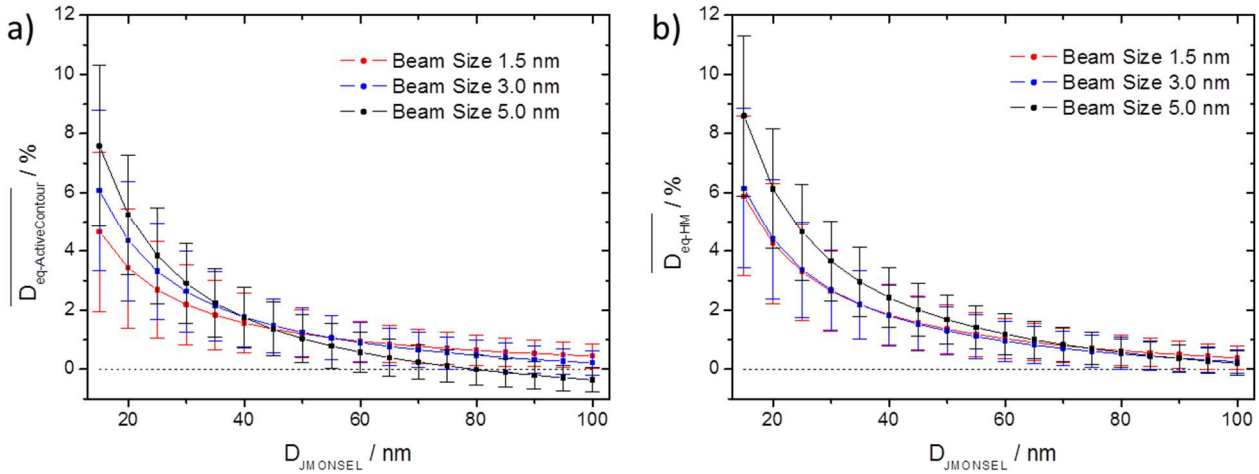

For both methods, the relative differences, $\overline{D_{eq-ActiveContour}}$ and $\overline{D_{eq-HM}}$, are systematically positive. This means that using $D_{eq\text{-}HM}$ and $D_{eq\text{-}ActiveContour}$, directly measured from profiles, for determining the smallest nanoparticle size implies errors and tends to underestimate their dimensions. This systematic discrepancy with respect to input value, $D_{JMONSEL}$, is observed, regardless e-beam width, for nanoparticle diameter below 70 nm and 85 nm for Active Contour and half-maximum segmentation methods, respectively. Moreover, this discrepancy increases with the reduction of nanoparticle size.

These differences can be explained by investigating SE profiles obtained with JMONSEL for various nanoparticle sizes. The *Figure 7* reports several profiles of nanoparticles with sizes ranging from 20 nm to 100 nm. Changes of profile shape occur when NP size increases. For a 20 nm size, the profile shows a maximum with a single peak whereas the signal is splitted in two peaks between 40 nm and 100 nm. Furthermore, in this range, a minimum in SE yield is observed between both peaks.

Figure 7 : SE profiles of silica nanoparticles calculated with JMONSEL with an input value of the parameter, $D_{JMONSEL}$, ranged from 20 nm to 100 nm.

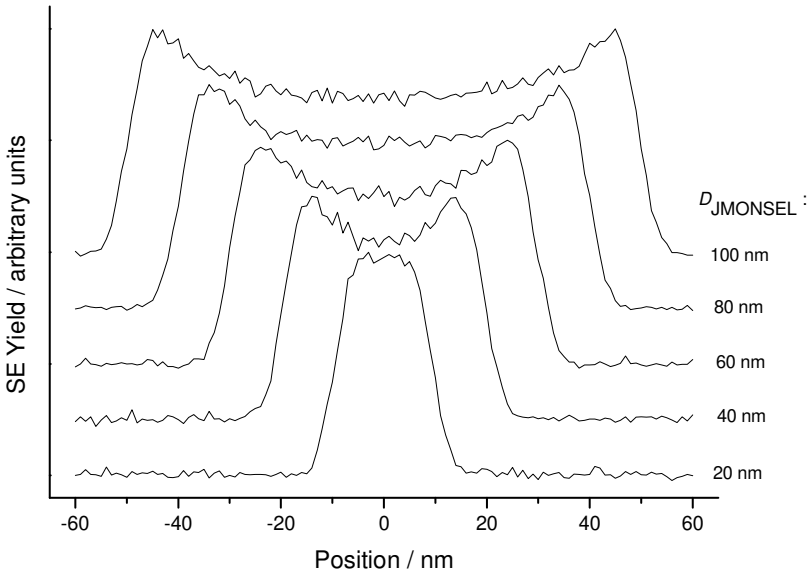

In order to understand this behavior, it important to get back to the interaction mechanisms between the SEM e-beam with a Gaussian shape and spherical nanoparticles of varying sizes.

Two different SE profiles of silica NP with $D_{JMONSEL}$ equal to 90 nm and 20 nm are presented in *Figure 8* and *Figure 9*, respectively. In each Figure, the position noted 1 corresponds to the boundaries of the nanoparticle and theoretically the distance between both boundaries is the NP real diameter and is equal to input value, D_{JMONSEL}.

Regarding the 90 nm size (*Figure 8*), the secondary electron yield at NP boundary (σ_b) appears to be close to that of the Full Width at Half-Minimum (FWHM) of the profile. However, for particle with $D_{JMONSEL}$ set as 20 nm, σ_b is significantly lower than this value inducing a notable discrepancy between $D_{eq\text{-}HM}$ and D_{JMONSEL}. This difference of the profile shape between large and small particles can be due to the combination of two parameters: the inelastic mean free path (IMFP), corresponding to the average distance needed to create a SE, that has been found to be equal to 7.0 nm for primary electron energy equal to 3000 eV in silica [29,30,31,32,33] and the maximum escape depth ($d_{max\text{-}escape}$) of SE generated inside silica which is about 10 nm to 20 nm [34].

For both particles, σ_b corresponds to the position 1 where only half of the electron beam is in contact with the particle, the other half only interact with the substrate (*Figure 9*).

The secondary electron profile shape of larger particles can be described as follows. First, the SE yield increases when the Gaussian electron beam scans the particle from the left to the right. At a distance from position 1 equal to twice the Gaussian beam standard deviation, σ, the maximum yield is reached. Beyond this point, the signal falls to a minimum value when the e-beam arrives at the NP center. Indeed, for large particles, the NP real radius is significantly larger than $d_{max\text{-}escape}$, consequently the SE created at a depth greater than $d_{max\text{-}escape}$ can't escape from the particle and a trapping area can be defined as shown in *Figure 8*. Because of the shape of the primary

electron/NP interaction volume, more and more SE are trapped in this area as the electron beam moves closer to the center of the particle. Therefore, a minimum yield is reached at the NP center where a large part of the generated SE are trapped in this central area as shown on the position 2 of *Figure 8*.

For large particles, σ_b is close to the yield at FWHM, giving $D_{\text{eq-HM}}$ equals to $D_{JMONSEL}$. At this position noted 1, half of the electron beam is in contact with the particle. As shown in *Figure 8*, almost every SE is created near to the particle surface. Thus, regarding these generated SE, the probability of escaping from the NP is only function of their direction. At maximum yield position, the effect is quite the same, however in this case all the primary electrons penetrate into the particle. Like in the case of the position 1, the majority of SE is generated near the NP edge and so can escape from the nanoparticle to be collected. Consequently, the difference in yield between these two positions is linked to the ratio number of primary electrons interacting with the particle, equal to 0.5.

For smaller particles, no signal drop is observed at the center of the particle. This behavior takes place when the NP real radius is close to $d_{max\text{-}escape}$. In this case, all secondary electrons generated within the particle can extract from it and be collected by the In-Lens detector within SEM chamber. As a result, the SE yield is related to the number of SE created and thus to the quantity of crossed material (*Figure 9*).

The difference observed between $D_{JMONSEL}$ and $D_{\text{eq-HM}}$ for small particles can be also explained regarding IMFP and SE escape depth. Indeed, even if the ratio of the number of primary electrons penetrating inside the particle should be 0.5 between σ_b and maximum yield positions, similarly to the larger ones, a part of primary electrons may not generate SE because the distance possibly crossed through the nanoparticle is shorter than IMFP. As shown in *Figure 9*. This is especially the case when the e-beam is located near to the position 1. As a consequence, for the smaller particles, the ratio between the maximum SE yield on the profile and σ_b is lower than 0.5 leading to a discrepancy between $D_{JMONSEL}$ and $D_{\text{eq-HM}}$. The results obtained with the ACTIVE CONTOUR method are similar because $D_{eq\text{-}ActiveContour}$ is by definition very close to $D_{\text{eq-HM}}$.

Figure 8: SE profile of silica NP with $D_{JMONSEL}$ set as 90 nm. The Gaussian-shaped electron beam standard deviation has been set to 3 nm. Representation of the primary (blue lines) and secondary (red lines) electrons trajectories at positions 1 and 2 on the SE profile.

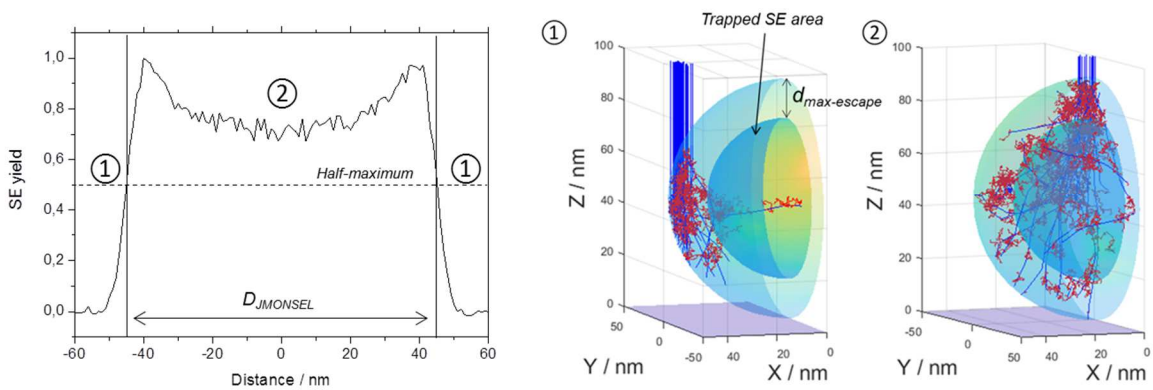

Figure 9: SE profile of silica NP with $D_{JMONSEL}$ set as 20 nm. The electron beam standard deviation has been set to 3 nm. Representation of the distance possibly crossed by the primary electron compared to IMFP at positions 1 and 2 on the SE profile.

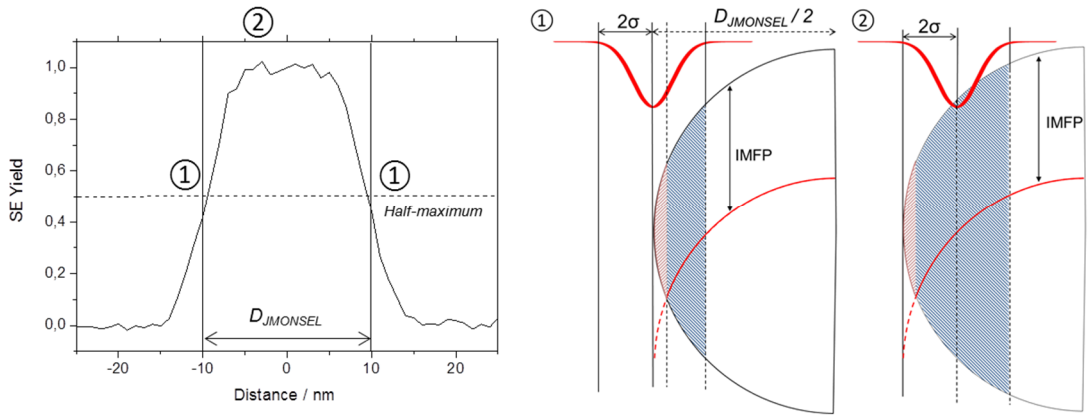

3.1.2. Comparison between the three methods

The objective of this section is to demonstrate the interest of using the $D_{eq\text{-}CurveCrossing}$ parameter to determine the spherical-like NP size.

The different defined D_{eq} have been calculated through JMONSEL simulated profiles. For an accelerating voltage equal to 3 kV and beam size equal to 3 nm, several line scans of silica NP with diameter ranging from 15 nm to 100 nm have been simulated. For each line scan, $D_{eq\text{-}CurveCrossing}$, $D_{eq\text{-}ActiveContour}$ and $D_{eq\text{-}HM}$ have been measured following methods describes in section 2.4.1 and compared with theoretical NP diameter ($D_{JMONSEL}$), input parameter introduced in the Monte Carlo model. The differences between $D_{JMONSEL}$ and D_{eq}, determined by using the three different segmentation methods, as a function of $D_{JMONSEL}$ are reported in *Figure 10*.

As observed in the previous section, results are quite similar for both methods, Active Contour and Half Maximum, with a discrepancy which is observed over the full nanoscale range and which tends to decrease when $D_{JMONSEL}$ increases, i.e., when the NP size increases. The maximum discrepancy observed for both techniques has been found to be roughly 6 %. In comparison, by using "Curve-crossing" method, the observed discrepancy is zero or close to zero (do not exceed 0.5 %), by considering uncertainties on the whole nanometer scale range. Therefore, these results demonstrate that $D_{eq\text{-}CurveCrossing}$ is the most reliable parameter for defining the nanoparticle size because its value is: (i) the closest to real size of the nanoparticle, (ii) not NP size-dependent and (iii) independent of the e-beam size.

Figure 10: Relative difference $\overline{\boldsymbol{D_{eq}}}$ determined using "Curve-crossing", Active Contour and Half Maximum segmentation techniques compared with $D_{JMONSEL}$ for silica particles with diameter ranging from 15 nm to 100 nm. Electron beam standard deviation has been set to 3 nm for all measurements.

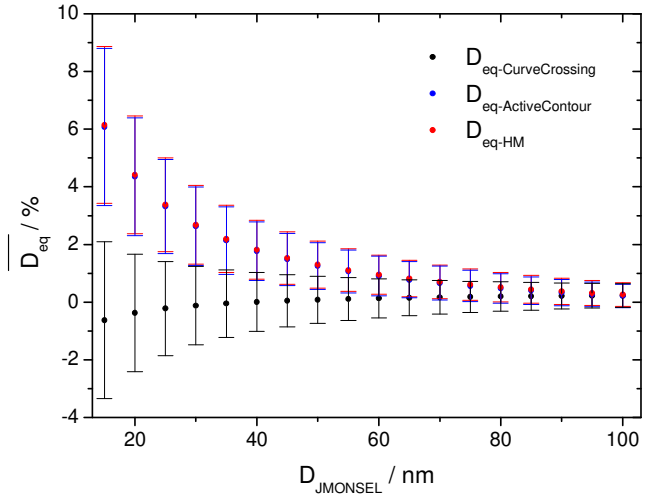

3.2. $D_{modal\text{-}eq}$ measurement and uncertainty evaluation of silica reference particle population for the three segmentation methods

3.2.1. Determination of the $D_{modal\text{-}eq}$ of silica reference particle population

The three methods used for determining NP size from a SEM profiles have been tested on a reference nanomaterial and compare with each other. SEM measurements have been performed on FD-101b silica reference nanoparticles deposited on silicon substrate following protocol presented in section 2.1. In order to have a sufficiently representative population of the sample, 200 isolated NP have been images using SEM parameters detailed in section 2.3.1. Then, the three segmentation methods have been applied on the images. Thus, for the same set of NP, the size distribution histograms of D_{eq} regarding both segmentation methods and calculated on 200 FD-101b particles were built and are presented in *Figure 11*. The modal diameter values of $D_{eq\text{-}HM}$, $D_{eq\text{-}ActiveContour}$ and $D_{eq\text{-}CurveCrossing}$ have been found to be 81.0 nm, 82.5 nm and 82.5 nm, respectively. As a reminder, the certified modal area equivalent diameter is given to be equal to (83.7 ± 2.2) nm (k = 2).

Figure 11: Histogram of size distribution of FD-101b NP built from SEM measurements using (a) Half Maximum, (b) Active Contour, (c) "Curve-crossing" segmentation method

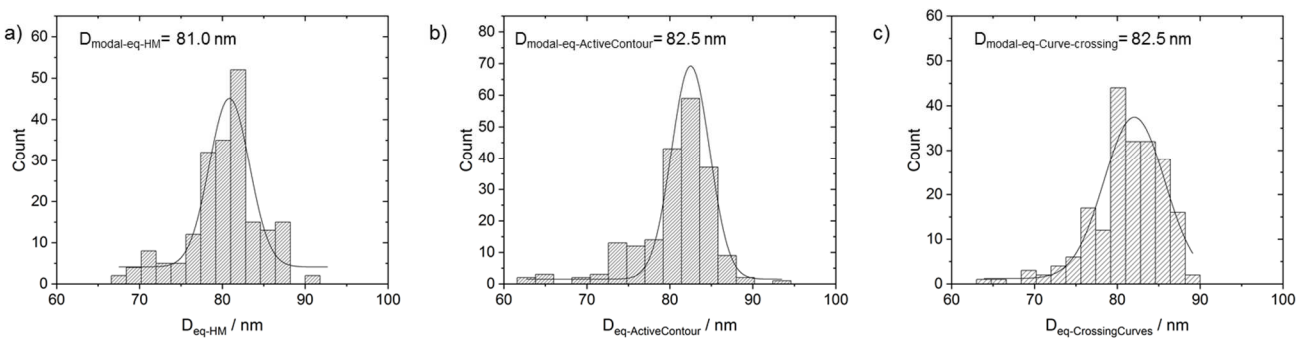

3.2.2. Uncertainty evaluation

The uncertainty budget linked to the measurement of $D_{\text{modal-eq}}$ of NP population using FWHM segmentation method had been previously evaluated in [3]. As a reminder, an in-depth study, using Ishikawa's method had been made on possible error sources. The main sources are the following: beam-width, repeatability, magnification, reproducibility between operators, pixel size, and calibration (see [3] for more details on the methods used to determine each contribution to the final uncertainty budget).

As the method used for locating NP on the image is different between this study and that conduct in [3], several contributions need to be reconsidered. Indeed, in previous study, particle counting is done by the operator using a Yes/No button. In this paper, the NP selection is performed automatically. Thus, the reproducibility of the measurements between operators does not contribute to the uncertainty budget. Furthermore, the uncertainty linked to the calibration is directly given by the FD-101b reference material calibration certificate and is equal to 1.1 nm (k = 1).

The repeatability of the $D_{modal\text{-}eq\text{-}HM}$ measurement of a population of 200 NP has been evaluated using FD-101b NP. $D_{modal\text{-}eq\text{-}HM}$ is calculated from a series of images randomly taken on the whole surface of the sample. The mean value between the NP populations for the three measurements has been found to be 81.1 nm, with a standard deviation of 0.5 nm. The uncertainty budget associated with the measurement of $D_{\text{modal-eq-HM}}$ is presented in *Table 1*.

Table 1: Uncertainty budget for the $D_{modal\text{-}eq\text{-}HM}$ of FD-101b particles

Source	Type of evaluation	Unit	Value	Standard uncertainty u_i	Sensitivity coefficient c_i	$c_i * u_i$	$c_i^2 * u_i^2$	Contribution / %
Beam Width – FD-101b	B	nm	0	1.7	1	1.7	2.89	65.41
Calibration – FD-101b	B	nm	0	1.1	1	1.1	1.21	27.39
Repeatability – FD-101b	A	nm	0	0.5	1	0.5	0.25	5.66
Magnification – FD-101b	B	nm	0	0.26	1	0.26	0.07	1.53
Pixel Size	A	-	-0.3215	0.014	1.4	0.02	0.00	0.01
				$D_{\text{modal-eq-corrected}}$	80.7	Variance	4.42	nm²
						Standard uncertainty	2.10	nm
						k	2	
						Expanded uncertainty	4.2	nm

As a result, $D_{modal\text{-}eq\text{-}HM}$ taking into account the error sources has been found to be (80.7 ± 4.2) nm (k = 2). The main component of the uncertainty budget corresponds to beam width and contributes for 65% of the expanded uncertainty. The uncertainty linked to the calibration represents about 27 %. Others components can be considered as minor as the sum of its contribution reaches 8 % of the expanded uncertainty.

Similarly, the $D_{\text{modal-eq}}$ uncertainty budget linked to FD-101b NP population using Active Contour can be established. The components are assumed to be the same that for $D_{\text{modal-eq-HM}}$ uncertainty evaluation. The repeatability of the $D_{modal\text{-}eq\text{-}ActiveContour}$ measurement has been calculated on the same populations similarly to the FWHM segmentation method (three series of 200 NP). For the three measurements, the mean $D_{modal\text{-}eq\text{-}ActiveContour}$ has been found to be 81.4 nm, with a 0.6 nm standard deviation. The uncertainty budget linked to the $D_{\text{modal-eq-ActiveContour}}$ measurement is presented in *Table 2*.

Table 2: Uncertainty budget for the $D_{modal\text{-}eq\text{-}ActiveContour}$ of FD-101b particles

Source	Type of evaluation	Unit	Value	Standard uncertainty u_i	Sensitivity coefficient c_i	$c_i * u_i$	$c_i^2 * u_i^2$	Contribution / %
Beam Width – FD-101b	B	nm	0	1.7	1	1.7	2.89	63.83
Calibration – FD-101b	B	nm	0	1.1	1	1.1	1.21	26.72
Repeatability – FD-101b	A	nm	0	0.6	1	0.6	0.36	7.95
Magnification – FD-101b	B	nm	0	0.26	1	0.26	0.07	1.49
Pixel Size	A	-	-0.3215	0.014	1.4	0.02	0.00	0.01
				$D_{\text{modal-eq-corrected}}$	80.9	Variance	4.53	nm²
						Standard uncertainty	2.13	nm
						k	2	
						Expanded uncertainty	4.26	nm

$D_{modal\text{-}eq\text{-}ActiveContour}$ taking into account the error sources has been found to be (80.9 ± 4.3) nm (k = 2).

The $D_{\text{modal-eq}}$ uncertainty budget corresponding to FD-101b NP population using "Curve-crossing" method has been evaluated as well. Unlike FWMH and Active Contour segmentation method, the contribution of beam width is null because the position of the intersection point is independent of the electron beam size. The repeatability of the $D_{modal\text{-}eq\text{-}CurveCrossing}$ measurement has also been evaluated on the same populations similarly to FWHM and Active Contour segmentation methods. For the three measurements, the mean $D_{modal\text{-}eq\text{-}CurveCrossing}$ is equal to 83.0 nm, with a 0.6 nm standard deviation.

However, another new component has been taken into account. Indeed, the "Curve-Crossing" method is based on the merger of several thumbnails of the same NP taken at different beam sizes. Thus, in order to be correctly overlaid, thumbnails are extracted and centered on the centroids of the indexed NP on the binary image created by using a rough threshold. However, several phenomena can generate a shift between the real NP centroid and the centroid deduced from binary image. For example, electron beam aberrations or threshold issues may modify the NP centroid positions on the binary image and misalign the thumbnail centroids between focused and defocused images. In order to evaluate the influence of this misalignment on the measurement of $D_{eq\text{-}CurveCrossing}$, some thumbnails of the same NP have been voluntarily shifted. Thus, 81 different combinations have been tested. A combination corresponds to the thumbnail shift by one or two pixels along X or Y directions. The

resulting standard deviation image and $D_{eq\text{-}CurveCrossing}$ are then calculated for each combination. From the 81 combinations, the standard deviation among all results has been found to be 0.1 nm for a single NP.

Table 3: Uncertainty budget for the $D_{modal\text{-}eq\text{-}CurveCrossing}$ of FD-101b particles

Source	Type of evaluation	Unit	Value	Standard uncertainty u_i	Sensitivity coefficient c_i	$c_i * u_i$	$c_i^2 * u_i^2$	Contribution / %
Calibration – FD-101b	B	nm	0	1.1	1	1.1	1.21	73.42
Repeatability – FD-101b	A	nm	0	0.6	1	0.6	0.36	21.84
Magnification – FD-101b	B	nm	0	0.26	1	0.26	0.07	4.10
Centroid misalignment – FD-101b	A	nm	0	0.1	1	0.1	0.01	0.61
Pixel Size	A	-	-0.3215	0.014	1.4	0.02	0.00	0.02
				$D_{modal\text{-}eq\text{-}corrected}$	82.5	Variance	1.65	nm²
						Standard uncertainty	1.28	nm
						k	2	
						Expanded uncertainty	2.57	nm

Finally, $D_{modal\text{-}eq\text{-}CurveCrossing}$ has been found to be (82.5 ± 2.6) nm ($k = 2$) and the main contribution to the uncertainty budget is the uncertainty linked to the calibration (73 %).

In conclusion, the $D_{modal\text{-}eq}$ of FD101b reference silica population has been evaluated using the three segmentation methods. As observed using Monte Carlo modeling, results are quite similar regardless the method used for this particular size. The modal diameter values of $D_{eq\text{-}HM}$, $D_{eq\text{-}ActiveContour}$ and $D_{eq\text{-}CurveCrossing}$, determined by averaging three populations of 200 NP, have been found to be 80.7 nm, 80.9 nm and 82.5 nm, respectively.

These results must be associated with the uncertainty budget established for each segmentation method. Thus, regarding the modal diameter values, $D_{modal\text{-}eq\text{-}HM}$ and $D_{modal\text{-}eq\text{-}ActiveContour}$, the expanded uncertainty (k = 2) is estimated to be 4.2 nm and 4.3 nm, respectively. These values have been established by assessing the effect of various imaging parameters on D_{eq} measurements by SEM. However, the uncertainty linked to the beam width has been found to be the most influential parameter for both methods (more than 60 %). Thus, as the beam width uncertainty does not contribute to the uncertainty budget associated with the measurement of $D_{modal\text{-}eq\text{-}CurveCrossing}$, this latter can be reduced to 2.6 nm (k = 2) as detailed in 3.2.2. The comparison of $D_{modal\text{-}eq\text{-}CurveCrossing}$, $D_{modal\text{-}eq\text{-}ActiveContour}$ and $D_{modal\text{-}eq\text{-}HM}$ values with the FD-101b modal area equivalent diameter reference value given by the calibration certificate, including their associated uncertainty is presented in *Figure 12*.

Figure 12: Comparison of $D_{modal\text{-}eq\text{-}CurveCrossing}$, $D_{modal\text{-}eq\text{-}ActiveContour}$ and $D_{modal\text{-}eq\text{-}HM}$ values, calculated on 200 FD-101b NP, with reference value given by the calibration certificate.

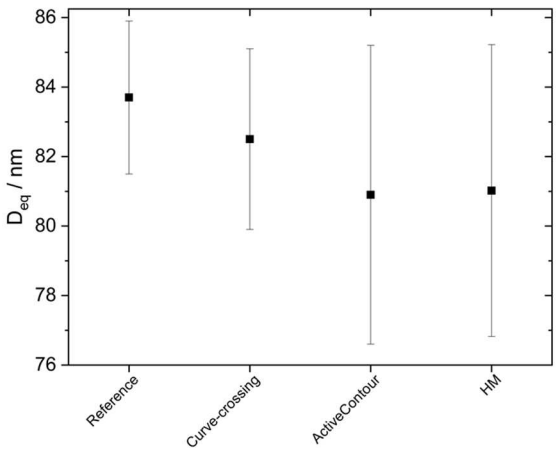

4. Conclusion

A novel approach to extract the NP diameter from a set of SEM images has been proposed. The method is based on the observation that, by varying the electron beam size, the secondary electron profiles crosses each other at a single point near to the NP boundary.

Firstly, the effect of electron beam size on classical segmentation methods (Active Contour and binarization at Half Maximum) has been evaluated through modelling. Monte Carlo modelling (JMONSEL) demonstrates that these segmentation methods are sensitive to electron beam size. Furthermore, systematic errors have been observed for nanoparticles smaller than roughly 80 nm. A nano-effect has been even highlighted because the discrepancy between the measurements carried out with these both conventional methods and the real size increases when the NP size decreases.

Then a theoretical study using Monte Carlo modelling has been performed in order to evaluate the feasibility of the method. From SE profiles simulated at different beam size, it has been shown that it was possible to extract mathematically this "Curve-crossing" point using a standard deviation calculation. Moreover, simulated profiles have shown that curves cross each other near to the NP boundary, and this, whatever particle size. A comparison of all methods studied here show that the discrepancies between the simulated and measured diameter are lower for the "Curve-crossing" method.

This method has also been tested experimentally on references silica particle (FD101b). A Matlab routine has been used on SEM images taken on the same area by varying focal distance to extract NP boundaries using "Curve-crossing" method. The comparison of the modal diameter values of $D_{eq\text{-}CurveCrossing}$, $D_{eq\text{-}ActiveContour}$ and $D_{eq\text{-}HM}$ with FD-101b reference value confirms observations made during Monte Carlo modelling.

One of the main advantages of this method is to not be influenced by the beam width, which is the most important contribution to the uncertainty budget for the measurement of NP by SEM. Thus, the expanded uncertainty, equal to 4.2 nm (k = 2) for Half Maximum segmentation technique, is reduced to 2.6 nm (k = 2) with

this new method. However, one drawback of the method is that it requires at least three images with different focuses which is time consuming but it could be more user friendly if supplier would implement this method directly as a native function of the microscope.

Acknowledgements

The authors would like to thank Digital Surf SARL for providing them with Digital Surf's MountainsMap® licenses in the framework of the Digital Surf's Mount Shasta technical cooperation program. They also thank Dr. John Villarrubia for the fruitful discussions.

1

[1] H. Rauscher and al. 2015 Recommendations on a Revision of the EC Definition of Nanomaterial Based on Analytical Possibilities *NanoDefine Technical Report* **D7.10**

[2] Delvallée A, Feltin N, Ducourtieux S, Trabelsi M and Hochepied JF 2015 Direct comparison of AFM and SEM measurements on the same set of nanoparticles. *Meas. Sci. Technol.* **26**(8). https://doi.org/10.1088/0957-0233/26/8/085601

[3] Crouzier L, Delvallée A, Allard A, Devoille L, Ducourtieux S and Feltin N 2019 Methodology to evaluate the uncertainty associated with nanoparticle dimensional measurements by SEM *Meas. Sci. Technol* https://doi.org/10.1088/1361-6501/ab1495

[4] ISO 13322-1. Particle size analysis - Image analysis methods - Part 1: static image analysis methods. 2014

[5] De Temmerman PJ, Verleysen E, Lammertyn J and Mast J 2014 Semi-automatic size measurement of primary particles in aggregated nanomaterials by transmission electron microscopy *Powder Technology* **261** 191-200 https://doi.org/10.1016/j.powtec.2014.04.040

[6] Häßler-Grohne W, Hüser D, Johnsen K-P, Frase CG and Bosse H 2011 Current limitations of SEM and AFM metrology for the characterization of 3D nanostructures *Meas. Sci. Technol.* **22**(9). https://doi.org/10.1088/0957-0233/22/9/094003

[7] Frase CG, Buhr E and Dirscherl K 2007 CD characterization of nanostructures in SEM metrology *Meas. Sci. Technol.* **18** 510-19. https://doi.org/10.1088/0957-0233/18/2/S26

[8] Kass M, Witkin A and Terzopoulos D 1988 Snakes: Active contour models *Int J Comput Vis* **1** 321–331 https://doi.org/10.1007/BF00133570

[9] Fisker R, Carstensen JM, Hansen MF, Bødker F and Mørup S 2000 Estimation of nanoparticle size distributions by image analysis *Journal of Nanoparticle Research* **2** 267-277 https://doi.org/10.1023/A:1010023316775

[10] Postek MT, Keery WJ and Larrabee RD 1988 The Relationship Between Accelerating Voltage and Electron Detection Modes to Linewidth Measurement in an SEM *Scanning* **10** 10-18 https://doi.org/10.1002/sca.4950100104

[11] Carl Zeiss SMT – Nano Technology Systems Division. Detection Principle based on GEMINI Technology.

[12] Orloff J. 2008. Handbook of charged particle optics. New York: CRC Press. https://doi.org/10.1201/9781420045550

[13] Joy DC 2002 SMART – a program to measure SEM resolution and imaging performance *J. Microsc-Oxford* **208** 24-34. https://doi.org/10.1046/j.1365-2818.2002.01062.x

[14] Babin S, Gaevski M, Joy DC, Machin M and Martynov A 2006 Technique to automatically measure electron-beam diameter and astigmatism: BEAMETR *J. Vac. Sci. Technol. B* **24**(6). https://doi.org/10.1116/1.2387158

[15] Meli F, Klein T, Burh E, Frase CG, Gleber G, Krumrey M, Duta A, Duta S, Koperlainen V, Bellotti R, Picotto GB, Boyd RD, Cuenat A 2012 Traceable size determination of nanoparticles, a comparison among European metrology institute, *Meas. Sci. Technol.* **23**(12). https://doi.org/10.1088/0957-0233/23/12/125005

[16] Zou YB, Khan MSS, Li HM, Li YG and al 2018 Use of model-based library in critical dimensions measurement by CD-SEM *Measurement* **123** 150-62

https://doi.org/10.1016/j.measurement.2018.02.069

[17] Buhr E, Senftleben N, Klein T, Bergmann D, Gniesser D and al 2009 Characterization of nanoparticles by scanning electron microscopy n transmission mode *Meas. Sci. Technol.* **20**(8)
https://doi.org/10.1088/0957-0233/20/8/084025

[18] Xing Q 2016 Information or Resolution: Which Is Required From an SEM to Study Bulk Inorganic Materials ? *Scanning* **38** 864-79
https://doi.org/10.1002/sca.21336

[19] Ramaye Y, Kestens V, Braun A, Linsinger T, Held A and Roebben G 2014 Certification Report. The certification of equivalent diameters of a mixture of silica nanoparticles in aqueous solution : ERM® -FD101b. European Commission, Join Research Centre, Institute for Reference Materials and Measurements (IRMM)
http://dx.doi.org/10.2787/212519

[20] Ghilini F, Rodriguez González MC, Miñán AG, Pissinis D, Hernández Creus A and al 2018 Highly Stabilized Nanoparticles on Poly-$_L$-Lysine-Coated Oxidized Metals: A versatile Platform with Enhanced Antimicrobial Activity *ACS Appl. Mater. Interfaces* **10**(28) 23657-66
https://doi.org/10.1021/acsami.8b07529

[21] Eklöf J, Gschneidtner T, Lara-Avila S, Nygård K and Moth-Poulsen K 2016 Controlling deposition of nanoparticles by tuning surface charge of SiO_2 by surface modifications *RCS Adv.* 6(106) 104246-53
https://doi.org/10.1039/c6ra22412a

[22] Ritchie NWM 2005 A new Monte Carlo application for complex sample geometries *Surf. Interface Anal.* **37** 1006-1011
https://doi.org/10.1002/sia.2093

[23] Villarrubia JS, Vladár AE and Postek MT 2005 Scanning electron microscope dimensional metrology using a model-based library *Surf. Interface Anal.* **37** 951-958
https://doi.org/10.1002/sia.2087

[24] Villarrubia JS, Ritchie NWM and Lowney JR 2007 Monte Carlo modeling of secondary electron imaging in three dimensions *Proc. SPIE* **6518**
https://doi.org/10.1117/12.712353

[25] Villarrubia JS and Ding ZJ 2009 Sensitivity of SEM width measurements to model assumptions *Proc. SPIE* **7272**
https://doi.org/10.1117/12.814300

[26] Villarrubia JS, Vladár AE, Ming B, Kline RJ, Sunday DF and al 2015 Scanning electron microscope measurement of width and shape of 10 nm patterned lines using a JMONSEL-modeled library *Ultramicroscopy* **154** 15-28
https://doi.org/10.1016/j.ultramic.2015.01.004

[27] Griffin BJ 2011 A comparison of conventional Everhart-Thornley style and in-lens secondary electron detectors: a further variable in scanning electron microscopy *Scanning* **33**(3) 162-73
https://doi.org/10.1002/sca.20255

[28] Marturi N, Dembélé S and Piat N 2013 Depth and Shape Estimation from Focus in Scanning Electron Microscope For Micromanipulation *IEEE International Conference on Control, Automation, Robotics and Embedded systems (CARE)* at Jabalpur, India
https://doi.org/10.1109/CARE.2013.6733694

[29] Powell C J, Jablonski A 2000 Evaluation of electron inelastic mean free paths for selected elements and compounds *Surf. Interf. Anal.* 29
https://doi.org/10.1002/(SICI)1096-9918(200002)29:2%3C108::AID-SIA700%3E3.0.CO;2-4

[30] Tanuma S, Powell C J, Penn D R 1991 Calculations of electron inelastic mean free paths. III. Data for 15 inorganic compounds over the 50-2000 eV range *Surf. Interf. Anal.* 17: 927
https://doi.org/10.1002/sia.740171305

[31] Ashley J C, Anderson V E 1981 Interaction of low-energy electrons with silicon dioxide *J. Electron Spectrosc. Relat. Phenom.* 24(2) 127-147
https://doi.org/10.1016/0368-2048(81)80001-1

[32] Akkerman A, Boutboul T, Breskin A, Chechik R, Gibrekhterman A, Lifshitz Y 1996 Inelastic Electron Interactions in the Energy Range 50 eV to 10 keV in Insulators: Alkali Halides and Metal Oxides *Phys. Stat. Solidi B* 198: 769
https://doi.org/10.1002/pssb.2221980222

[33] Kwei C M, Chen Y F, Tung C J, Wang J P 1993 Electron inelastic mean free paths for plasmon excitations and interband transitions *Surface Science* 293(3) 202-210
https://doi.org/10.1016/0039-6028(93)90314-A

[34] Kanaya K, Ono S, Ishigaki F 1978 Secondary electron emission from insulators *J. Phys. D: Appl. Phys.* 11 2425
https://doi.org/10.1088/0022-3727/11/17/015